Computation of the dendritic operating state at large supercoolings by the phase field model

Shun-Lien Wang* and Robert F. Sekerka
Department of Physics, Carnegie Mellon University, Pittsburgh, Pennsylvania 15213
(Received 4 August 1995)

The phase field model in two dimensions is used to calculate numerically the operating states (tip velocity v and tip radius ρ) of dendrites grown from pure melts. At large supercoolings, a dendrite has a nearly hyperbolic envelope close to its tip, as opposed to being nearly parabolic, as at small supercoolings. The corresponding tip radius increases with supercooling for anisotropy only in surface tension, decreases for anisotropy only in interface kinetics, and displays a mixture of these behaviors when both are anisotropic. The growth velocity is found to increase as a power law with increasing supercooling, to decrease with increased effect of interface kinetics, and to increase with increased anisotropies of surface tension and interface kinetics. Interface kinetics are shown to have a strong effect in that a smaller kinetic coefficient leads to a smaller velocity and a larger tip radius at a given supercooling. The Péclet number $P = v\rho/(2\kappa)$, where κ is the thermal diffusivity, is found to increase with supercooling while the opposite is true for the selection parameter $\sigma = 2\kappa d_0/(v\rho^2)$, where d_0 is the capillary length. The dependencies of P and σ on interface kinetics are found to be influenced strongly by anisotropies.

PACS number(s): 68.70.+w, 47.54.+r, 64.70.Dv, 68.10.Gw

I. INTRODUCTION

Theoretical research on the issues of dendritic growth patterns and the selection of the tip operating state (i.e., the tip growth velocity v and the corresponding radius of curvature ρ) has been very rich in the literature. (See [1] for a recent review.) The growth of crystals from pure melts is generally recognized to be determined by the interplay of heat transport in the bulk phases and, at the crystal-melt interface, the presence of excess interfacial free energy, which shifts the local thermodynamic equilibrium (capillary effect), and the dynamical rearrangement of atoms or molecules from one phase to the other (interface kinetics). Mathematically, the growth process is modeled by a moving boundary problem, often referred to as the modified Stefan problem. The temperature fields in each phase satisfy a heat diffusion equation and are coupled at the unknown crystal-melt interface through two boundary conditions that account for conservation of energy and relate the interface temperature to the thermodynamic melting point by accounting for the effects of capillarity and interface kinetics.

In the absence of capillary and interface kinetic effects, i.e., when the interface temperature is assumed to be constant and equal to the equilibrium melting point, a steady-state solution of this free boundary problem was first obtained by Ivantsov [2]. He found steady-state solutions for a "needle crystal" (branchless dendrite) in the shape of a paraboloid of revolution (three dimensional) or a parabola (two dimensional) moving at constant velocity. In two dimensions, his solution leads to the relationship

$$S = \sqrt{\pi P}\exp(P)\mathrm{erfc}(\sqrt{P}), \tag{1}$$

where S is the dimensionless supercooling

$$S = \frac{T_M - T_\infty}{L_0/c} \tag{2}$$

and P is the dimensionless Péclet number

$$P = \frac{v\rho}{2\kappa}. \tag{3}$$

Here T_M is the thermodynamic melting temperature, T_∞ is the temperature at far field, L_0 is the latent heat per unit volume, c is the volumetric heat capacity and κ is the thermal diffusivity of the melt. Here, erfc denotes the complementary error function. Thus, for Ivantsov's solutions, specification of the supercooling S will only determine the product of the growth velocity and tip radius rather than the individual quantities v and ρ.

Considerable effort in theoretical analysis has been directed toward understanding the unique dendrite operating state, mostly based on models that pertain to the steady state growth of a (branchless) Ivantsov dendrite. One important breakthrough on tip selection was the marginal stability criterion introduced by Langer and Müller-Krumbhaar [3,4]. They conjectured that the tip radius of the Ivantsov paraboloidal dendrite was essentially the marginal morphological stability wavelength according to the Mullins-Sekerka instability theory [5]. This conjecture then led to a prediction that a selection parameter σ, defined as

$$\sigma = \frac{2\kappa d_0}{v\rho^2} \tag{4}$$

is a universal constant σ^*, equal to about 0.025 in the limit of small supercoolings. Here $d_0 = \gamma T_M c/L_0^2$ is the

*Present address: Technology Modeling Associates, Inc., 3950 Fabian Way, Palo Alto, CA 94303-4605.

capillary length, proportional to the surface tension γ. This condition, combined with Eq. (1), determines the unique dynamical operating state. A more recent theory, called microscopic solvability theory, showed that there is no steady-state solution for a parabolic dendrite unless the anisotropy of surface tension is accounted for, which leads to a discrete set of steady-state solutions. Among those solutions, only one is stable with respect to small perturbations on the tip. This solution, which corresponds to the *solvability condition*, gives a unique value for the tip radius. Accordingly, the value of σ is predicted to be a function of the anisotropy. For instance, in the limit of very small anisotropies and negligible interface kinetics, σ varies as the 7/4 power of the anisotropy of surface tension, which has a specific value for a given material. Thus the macroscopic form of a dendrite is determined by the microscopic length scale of capillarity, characteristic of surface tension and typically of the order of angstroms, and its associated anisotropy. The extension of this solvability theory has been explored in a variety of situations. For instance, some models include interface kinetics and some consider the effects of varying the Péclet number, which results in various functional forms for the selection parameter σ [6–12]. Some reviews of the recent developments of microscopic solvability theory can be found in [13–16].

Note that once P are σ are known, v and ρ can be calculated by the equations

$$v = \frac{2\kappa}{d_0}\sigma P^2, \tag{5}$$

$$\rho = \frac{d_0}{\sigma}\frac{1}{P}. \tag{6}$$

In other words, to obtain the dendritic operating state for a given value of S, it is necessary to determine both σ and P. However, although it is understood that anisotropy is crucial in determining the selection parameter σ, most studies, such as those in the framework of microscopic solvability theory, assume that the Péclet number is determined solely by supercooling via Eq. (1), independent of the effects of capillarity and interface kinetics as well as their anisotropies. In actuality, however, this may not be the case, in particular at large supercoolings when interface kinetic effects become significant.

The predictions of σ, however, are neither confirmed nor contradicted by experimental data. For instance, highly purified succinonitrile (SCN) was reported [17] to have nearly identical values of $\sigma = 0.0192$ for a range of supercoolings, which is roughly in agreement with the marginal stability prediction. Reports on pivalic acid (PVA) [18] show that $1/\sigma$ increases nearly linearly with supercooling. For PVA, the resulting dendrites display strongly anisotropic morphologies that are characteristic of kinetic influence and the anisotropy of surface tension is ten times stronger than for SCN. Growth of krypton and xenon studied by Bilgram *et al.* [19,20] showed σ to be decreasing somewhat with supercooling. Since the surface tension of rare-gas solids was shown to be nearly isotropic [21], anisotropic interface kinetics was suggested to play an important role. Recent experimental data for nickel [22] displays a discontinuity in the dependence of growth velocity with the supercooling. The authors explained this by appealing to a kinetic effect. A more detailed comparison of the theoretical prediction of σ with experimental data can be found in [1] and [23].

For a better understanding of dendritic growth, it is therefore essential to consider heat diffusion and the effects of capillarity and interface kinetics simultaneously, as well as their anisotropies. Since models of dendritic growth are inherently nonlinear, analytic methods are not applicable and numerical approaches are usually necessary.

The classical numerical approach is to solve the modified Stefan problem. However, this is a difficult free boundary problem to implement numerically, since explicit tracking of the moving interface is necessary. An alternative numerical method can be based on the phase field model, which was adopted independently for the crystallization problem by Langer [24,25] and by Collins and Levine [26]. In this model, a phase field $\phi(\mathbf{x}, t)$ is postulated to identify the phase. The variable ϕ assumes a representative value in each phase, say, 0 in the solid and 1 in the liquid, and changes rapidly but continuously over a thin transition layer near the solid-liquid interface. Explicit interface tracking is thus replaced by two coupled partial differential equations, one for the temperature field and another for the phase field. Since its introduction to the crystallization problem, the physical and mathematical basis of the phase field model has been studied extensively [27–49].

Moreover, the operating state and interface morphology of dendrites have been studied via the phase field in both two [50–56] and three [57] dimensions.

In our previous study [46], we developed a self-consistent nonisothermal version of the phase field model based on an entropy functional [44], distinguished from others in that it guarantees positive *local* entropy production. Moreover, it was shown that the parameters that control anisotropies of interfacial properties can be specified quantitatively [47]. The utility of the phase field model is thus strengthened, since it allows us to control *independently* the anisotropies as well as the strengths of surface tension and interface kinetics. As a result, the roles played by these parameters in dendritic growth can be studied extensively.

In this paper, we use the phase field model to study dendritic growth during solidification from a pure substance. The main objective is to calculate dendritic operating states that are quantitatively independent of *computational* parameters.

We applied finite-difference methods on a two-dimensional uniform grid to solve the phase field equations. Details of our numerical methods are discussed elsewhere [58]. In that paper, we consider carefully the length scale differences among the capillary length, the interface thickness, the tip radius, and the computational domain size. We show that results independent of computational parameters can only be obtained at very large supercoolings. Presumedly, one could employ adaptive moving grids to get results at lower supercoolings, but in some sense such algorithms run counter to the advantage

of the phase field model, which is supposed to eliminate interface tracking. A range of values of anisotropy is adopted by considering affordable computational times. Generally speaking, these values of anisotropy are higher than those for which analytical analyses are applicable.

This paper is organized as follows. In Sec. II we summarize the formulation of the phase field model for solidification. Also included in this section is a brief description of the numerical implementation. Section III discusses the tip shape of a dendrite at large supercoolings. Section IV contains the quantitative values of the tip radius and tip velocity as functions of supercooling, surface kinetics, and anisotropies. Section V offers a discussion of our work and others.

II. PHASE FIELD MODEL

Consider a system of volume V in which a pure material undergoes a first-order phase transition between crystalline solid and liquid. For simplicity, we assume uniform density throughout the system and that there is no convection in the liquid.

By guaranteeing spatially local positive-entropy production for the system [46,47], the phase field model in two dimensions leads to a pair of coupled partial differential equations. The dimensionless temperature field $u = (T - T_M)/(T_M - T_\infty)$ is governed by

$$\frac{\partial u}{\partial t} + \frac{30\phi^2(1-\phi)^2}{S}\frac{\partial \phi}{\partial t} = \nabla^2 u, \tag{7}$$

which reduces to the heat equation in the region where $\phi = 0$ and 1, and the phase field is governed by

$$\frac{q(\theta)}{\bar{m}}\frac{\partial \phi}{\partial t} = F(\phi, u) + \nabla \cdot [B(\theta)\nabla\phi], \tag{8}$$

where

$$B(\theta) = \begin{pmatrix} r^2(\theta) & -r(\theta)r'(\theta) \\ r(\theta)r'(\theta) & r^2(\theta) \end{pmatrix} \tag{9}$$

and

$$F(\phi, u) = \frac{1}{\bar{\epsilon}^2}\phi(1-\phi)\left[\phi - \frac{1}{2} + 30\bar{\epsilon}\alpha S \times \frac{u}{1 + (L_0/cT_M)u}\phi(1-\phi)\right]. \tag{10}$$

Here lengths are scaled in units of the characteristic domain size w and time in units of w^2/κ. Both $\bar{\epsilon}$ and α are computational parameters: $\bar{\epsilon} = \tilde{\delta}/w$ is the ratio of the interface thickness parameter to the characteristic domain size and $\alpha = w/(6\sqrt{2}d_0)$, where d_0 is related to the strength of surface tension $\bar{\gamma}$ by $d_0 = \bar{\gamma}T_M c/L_0^2$. By means of matched asymptotic expansions for $\bar{\epsilon} \to 0$ with α and $\bar{m}$ fixed (i.e., the interface tends to nearly zero thickness), two deductions can be made. First, the parameter $\bar{m}$ can be related to the strength $\bar{\mu}$ of a linear kinetic law of the form $v = \bar{\mu}(1+\delta_\mu \cos 4\theta)\delta T$, where δT is the interfacial undercooling, by the equation $\bar{m} = d_0/\rho_K$, where $\rho_K = ck/(\bar{\mu}L_0)$ is a kinetic length. Therefore, $\bar{m} = \bar{\mu}\bar{\gamma}T_M/(\kappa L_0)$ is completely determined by material parameters and is proportional to the kinetic coefficient. The smaller the value of $\bar{m}$, the more significant the interface kinetic effect compared to the capillary effect. The other deduction is that, with θ defined as the angle between the normal to the interface (defined asymptotically as the locus of $\phi = 1/2$) and a reference direction, presumed to be of crystallographic significance, i.e.,

$$\theta = \arctan\left(\frac{\phi_y}{\phi_x}\right)\Bigg|_{\phi=\text{const}}, \tag{11}$$

proper choices for the functions $r(\theta)$ and $q(\theta)$ enable independent control of the anisotropies of surface tension and interface kinetics [47]. As an example, which will be used in subsequent computations, we choose

$$r(\theta) = 1 + \delta_\gamma \cos(4\theta), \tag{12}$$

$$q(\theta) = \frac{1 + \delta_\gamma \cos(4\theta)}{1 + \delta_\mu \cos(4\theta)}. \tag{13}$$

This corresponds to the choices of fourfold anisotropic surface tension $\gamma(\theta) = \bar{\gamma}[1 + \delta_\gamma \cos(4\theta)]$ and fourfold anisotropic kinetic coefficient $\mu(\theta) = \bar{\mu}[1 + \delta_\mu \cos(4\theta)]$, where δ_γ and δ_μ are the corresponding strengths of anisotropy, respectively. As a result, the phase field model enables one to understand the separate effects that four physical parameters (S, $\bar{m}$, δ_γ, and δ_μ) have on the selection of the dendritic operating state.

To solve Eqs. (7) and (8), we applied finite-difference methods on a uniform grid. An alternating direction implicit method [59] is applied for Eq. (7) and an explicit Euler scheme is employed for Eq. (8). Due to the large differences among the length scales involved in dendritic growth (capillary length, interface thickness, dendrite tip radius, and computational system size) we have determined that results independent of computational parameters can be obtained for affordable computation times only at very large supercoolings ranging from 0.7 to 1.1 and strong anisotropies of several percent. Other details of the numerical algorithm and the selection for the proper range of supercooling are presented in [58].

Computational results are presented in the next two sections. We first address the tip shape of the dendrites at large supercoolings. This is followed by results for the calculated dimensionless growth velocity $\tilde{v} = v/(\kappa/d_0)$ and the dimensionless tip radius $\tilde{\rho} = \rho/d_0$ for a range of parameters S, $\bar{m}$, δ_γ, and δ_μ.

III. RESULTS FOR THE TIP SHAPES OF DENDRITES

Recently, Brener and Temkin [60] conjectured that dendrites at large supercoolings are "angular," i.e., instead of being parabolic cylinders, they would have planar sections far from the tip and the entire shape would be relatively branchless. Based on a boundary layer model, Brener and Temkin predict that this morpholog-

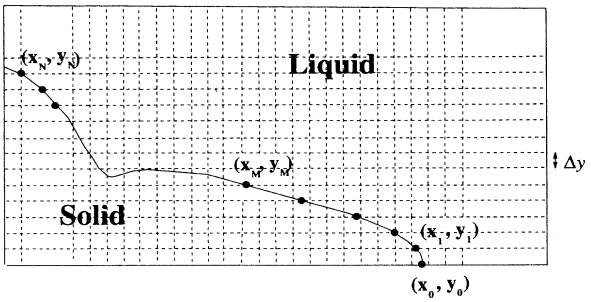

FIG. 1. Interface defined by the locus $\phi = 1/2$. Its position is estimated by the linear interpolation along the x direction from the values of ϕ at the mesh points located at equal intervals of y. The numbering starts from the bottom of the domain. The coordinate of the Mth point is $(x_M, M\Delta y)$, where Δy is the mesh size.

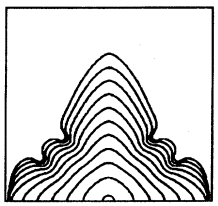

FIG. 2. Evolution of a dendrite with parameters $S = 0.8$, $\bar{m} = 0.1$, and $\delta_\gamma = \delta_\mu = 0.03$. The growth shapes are shown at time increments of 0.04 for time intervals 0.0-0.4.

ical transition (from parabola to angular) occurs for values of supercooling $S \geq 1$. We recognize that an angular shape is more nearly "hyperbolic" than parabolic, since a hyperbola resembles a parabola very near the tip but asymptotically approaches straight lines far from the tip. Our calculated results suggest that a hyperbolic shape may be incipient at large values of S, even for $S < 1$, as will be discussed in the following.

We define the interface by the locus $\phi(x, y, t) = 1/2$ and estimate its position by linear interpolation along the x direction from the values of ϕ at mesh points that occur at equal intervals of y. Thus the interface locus is represented by a series of data points (x_i, y_i) for $i = 0, \ldots, N$ as depicted in Fig. 1. We then compare the calculated locus of the dendritic tip to the *best*-fitting parabola (the one that gives the least-squares residue χ_p^2) and the *best* fitting hyperbola (the one which gives least squares residue χ_h^2). If $\chi_h^2 < \chi_p^2$, the shape of the dendrite is said to be more nearly hyperbolic than parabolic and vice versa.

A dendrite growing along the x axis will be the subject of our study. In general, a parabola is described by

$$x_p(y, a_0, a_2) = a_0 - a_2 y^2, \tag{14}$$

where a linear term in y does not appear because we have imposed a reflection symmetry in y. A general hyperbola is described by

$$x_h(y, b_0, b_1, b_2) = b_0 - b_1\sqrt{1 + y^2/b_2^2}. \tag{15}$$

Further, we impose one more constraint on Eq. (15) by forcing the fitted hyperbolic curve to pass through the point $(x_0, 0)$. As a result, $b_0 = b_1 + x_0$. This constraint will not be imposed on Eq. (14), however, for the following reason. If this condition is applied to Eq. (14), there will be only one free parameter a_2 left in Eq. (14) with the value of a_0 determined to be x_0. Because a quite general curve can be represented by a polynomial of large degree, the calculated residue may decrease when more terms are included. Thus the residues calculated by having two fitted coefficients, both a_0 and a_2 in Eq. (14), would be expected to be smaller, or at least as small, as for fitting with one coefficient a_2. Therefore, we choose to compare the residues with two free fitting parameters in each equation, Eq. (14) and Eq. (15). Note that Eq. (15) does not resemble a general polynomial of infinite degree; the coefficients of the series expansion of Eq. (15) are *mutually dependent* while the coefficients of a general polynomial are mutually independent.

The fitting parameters $a_{0,2}$ and $b_{1,2}$ are to be determined by minimizing the squared residues

$$\chi_p^2(a_0, a_2) = \sum_{i=0}^{M} [x_i - x_p(y_i, a_0, a_2)]^2, \tag{16}$$

$$\chi_h^2(b_1, b_2) = \sum_{i=1}^{M} [x_i - x_h(y_i, b_1, b_2)]^2 \tag{17}$$

separately, where M is the number of points used for fitting. Therefore, there is a total of $M + 1$ sampling points $(x_0 - x_M)$ to be fitted to Eq. (14) and M sampling points $(x_1 - x_M)$ to be fitted to Eq. (15). The data range of the sampling points is between 0 and MΔy along the y coordinate (see Fig. 1). The average least-squares residue is estimated by $\bar{\chi}_p^2 = \chi_p^2/(M-1)$ for $M > 1$ and $\bar{\chi}_h^2 = \chi_h^2/(M-2)$ for $M > 2$, respectively. [The value of $\chi_{p,h}^2$ is zero if only two sampling points are used for fitting to Eqs. (14) and (15).] Note that χ_h^2 depends nonlinearly on its fitted coefficients b_1 and b_2, so that the minimization requires an iterative procedure: Given trial values for the parameters, the procedure is iterated to improve the trial values until χ_h^2 stops (or effectively stops) decreasing.

Figure 2 shows a time sequence of dendritic shapes of the type that we analyzed at late times, after a steady state is reached near the dendrite tip. Figure 3 gives an example for the calculated results of $\sqrt{\bar{\chi}_h^2}$ and $\sqrt{\bar{\chi}_p^2}$, which we label "root-mean-square residue," as a function of the number of sampling points. The dimensional value of the mesh size is $\Delta y = 1.05\, d_0$. Since the tip radius of the parabola is related to a_2 by $\tilde{\rho} = 1/(2a_2)$ and to the radius of the hyperbola at the tip by $\tilde{\rho} = b_2^2/b_1$, the corresponding radii from each fit are calculated and presented in the figure. As may be observed, the value of the root-mean-square residue obtained by fitting to an hyperbola is smaller than by fitting to a parabola. When

M is small, the values of these residues are comparable to each other. This is reasonable since the geometries of the parabola and hyperbola are about the same very near the tip. When the value of M increases, the difference between the residues increases rapidly. The calculated values of tip radii from fitting to a parabola is significantly dependent on the number of sampling points while the results from fitting to a hyperbola results in relatively little change in the tip radius when the data range on the y coordinate is between 0 and $\tilde{\rho}$. Therefore, the result demonstrates that the region around the tip may be more nearly hyperbolic than parabolic, as shown in Fig. 4. As noted in our other paper [58] that deals with computational aspects of this study, we employed a rectangular domain to save computational time. This sharply affects growth in the y direction, but has negligible effect on growth in the x direction, including consideration of tip shape. Besides, the effects of a finite domain in the y direction would be expected to favor a parabolic shape, not a hyperbolic shape. On the other hand, the hyperbolic shape might be due to the incipient emergence of sidebranches, in real systems as well as in our calculations. Far back from the tip, a steady-state branchless "needle crystal" must tend to a parabola for $S < 1$; but our calculated shapes are finite in extent, even though the tip speed and radii of curvature become practically constant at sufficiently large times. In Fig. 2, for example, the first sidebranch occurs about 5–10 tip radii from the tip, but could influence the shape closer to the tip.

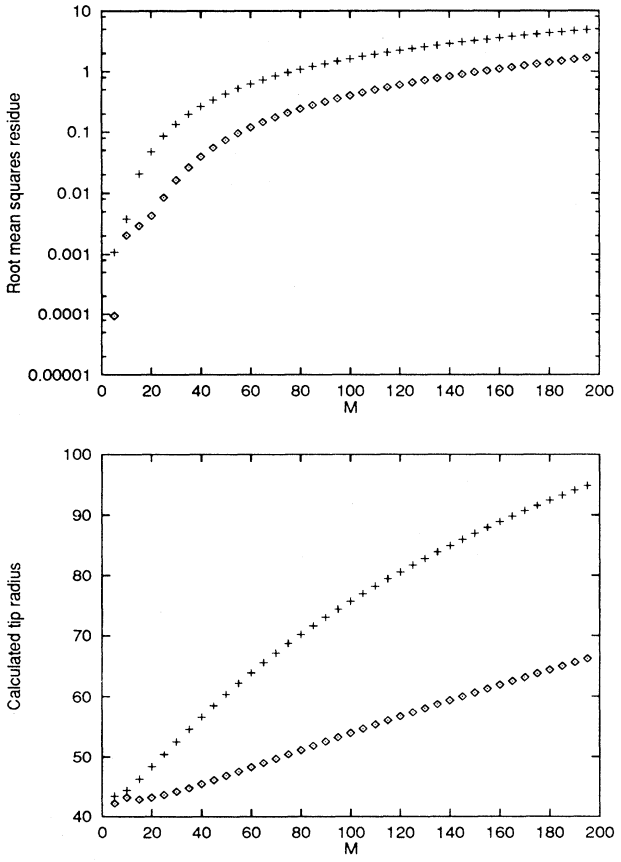

FIG. 3. Root-mean-square residue and calculated tip radii as a function of the number of fitting points. The fit is with respect to the locus of the interface of Fig. 2 at time 0.40. The crosses are for fitting to an parabola and the diamond marks are for fitting to a hyperbola. The unit for the residue and tip radius is d_0 and that for the grid size is $1.05d_0$.

IV. RESULTS FOR SELECTION OF THE OPERATING STATE

Below we present results for the calculated dimensionless growth velocity $\tilde{v} = v/(\kappa/d_0)$ and the dimensionless tip radius $\tilde{\rho} = \rho/d_0$ for a range of parameters S, δ_γ, δ_μ, and $\bar{m}$. We classify our results in terms of anisotropies of surface tension (δ_γ) and interface kinetics (δ_μ) as follows: case (i), $\delta_\gamma \neq 0$, and $\delta_\mu = 0$; case (ii), $\delta_\gamma = 0$, and $\delta_\mu \neq 0$; and case (iii), $\delta_\gamma \neq 0$, and $\delta_\mu \neq 0$.

In each classification, the variations of growth velocity and tip radius with S and $\bar{m}$ are studied. To understand quantitatively the influence of anisotropy on the selection of operating states, the variations of growth velocity and tip radius as a function of anisotropy are examined at fixed values of $S = 0.8$ and $\bar{m} = 0.1$ for each classification. These values of S and $\bar{m}$ were chosen on the basis of affordable computational time.

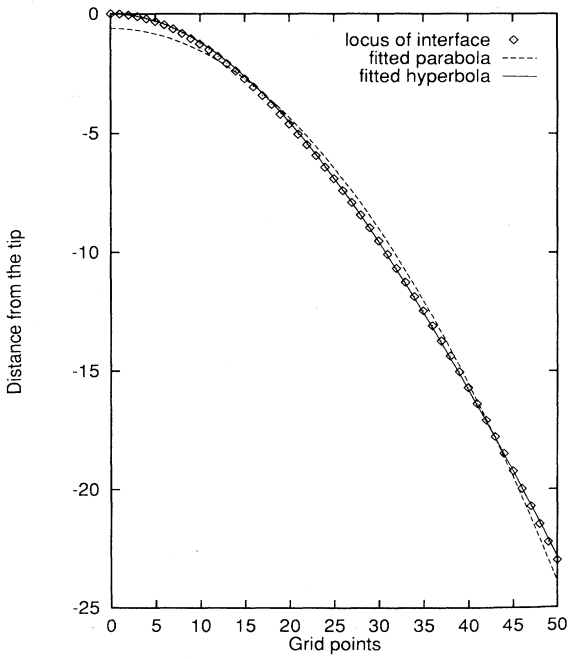

FIG. 4. Locus of the interface, Fig. 2 at time 0.36, compared to the best-fit hyperbolic curve and the best-fit parabolic curve, which are fit by using data points up to $M = 50$. The unit for the distance is d_0 and that for the grid size is $1.05d_0$.

In previous theoretical work, the Péclet number was assumed to be independent of $\bar{m}$ and anisotropy, whereas the selection parameter σ could be a function of S, $\bar{m}$, δ_γ, and δ_μ ([7]). This motivates us to examine, at large supercoolings, the behaviors of P and σ, in addition to $\tilde{v}$ and $\tilde{\rho}$, as functions of S, $\bar{m}$, δ_γ, and δ_μ.

The growth velocity and the tip radius are calculated in the following manner: Since our study showed that the shape of the dendrite is more nearly an hyperbola, we chose the value of the tip radius as that of an hyperbola best fitted by the data points that range from $0 \sim \tilde{\rho}$ on the y coordinate (see Sec. III), i.e. the point where $\tilde{\rho} \simeq 1.05M$, as in the diamond curve in Fig. 3. The tip velocity is derived by dividing the distance of propagation of the tip by each corresponding interval of time. Additionally, the temperature at the tip is also checked as a function of time. If the dendrite reaches a steady state, the temperature at the tip should remain at a constant value.

A. Case (i): Dendrites with $\delta_\gamma \neq 0$ and $\delta_\mu = 0$

In this section, we deal with dendrites that have anisotropy in the surface tension alone [Case (i)]. The computed values of $\tilde{v}$ as a function of S for $\bar{m} = 0.1$, $\delta_\mu = 0$, and three values of δ_γ are shown on a log-log plot in Fig. 5(a). From the velocity plot, it is evident that a power law exists and that $\delta_\gamma = 0.05$ leads to a higher velocity than $\delta_\gamma = 0.04$ or $\delta_\gamma = 0.03$. The exponent (b) of S for $\tilde{v}$ is given in Table I. There is about a 10% variation in the exponent of S from $\delta_\gamma = 0.03$ to 0.05.

The variation of the calculated values of $\tilde{v}$ with S for $\delta_\gamma = 0.05$ and $\bar{m} = 0.075$ is shown in Fig. 6(a), in which the results obtained for $\bar{m} = 0.1$ are also plotted for comparison. Again, a power-law-type relationship is deduced from the log-log plot. Also, a larger value of $\bar{m}$ is seen to lead to a larger value of $\tilde{v}$.

A graph of $\tilde{\rho}$ versus S for $\bar{m} = 0.1$ and three values of δ_γ is displayed in Fig. 5(b). We can make the following observations.

(a) There is a definite decrease of $\tilde{\rho}$ with increasing anisotropy.

(b) In contrast to the linear behavior between $\log \tilde{v}$ and $\log S$, there is no such linear dependence of $\log \tilde{\rho}$ on $\log S$.

TABLE I. Least-squares fit of the growth velocity $\tilde{v}$ as a function of supercooling S, $\log \tilde{v} = a + b \log S$.

δ_γ	δ_μ	$\bar{m}$	a	b
0.03	0	0.1	-1.71	2.78
0.04	0	0.1	-1.62	2.62
0.05	0	0.1	-1.55	2.55
0.05	0	0.075	-1.69	2.37

(c) At smaller supercoolings ($S \sim 0.75$), the value of $\tilde{\rho}$ does not change appreciably as supercooling increases. At larger supercoolings ($S > 1.0$), there is a notable increase in $\tilde{\rho}$ with increased supercooling. This increasing trend for $0.7 \leq S \leq 1.1$ is quite unexpected since the results obtained from experiments and from theoretical predictions that are carried out at very small supercoolings ($S \leq 0.1$) indicate that $\tilde{\rho}$ decreases with supercooling. This unusual dependence of $\tilde{\rho}$ on S is possibly due to the effect of *isotropic* interface kinetics.

(d) A comparison of the variation of $\tilde{\rho}$ for two different values of $\bar{m}$, plotted in Fig. 6(b), shows that the increase of $\tilde{\rho}$ with S is somewhat enhanced with a smaller value of $\bar{m}$, that is, with a stronger effect of interface kinetics.

Since $\tilde{v}$ decreases with $\bar{m}$ while $\tilde{\rho}$ increases with $\bar{m}$, further studies of the variations of $\tilde{v}$ and $\tilde{\rho}$ with S for values of $\bar{m}$ smaller than 0.075 (for example, for $\bar{m} = 0.05$) are not practical from a computational standpoint (due to the requirements of a larger computational domain and a much longer interval of computation time). Consequently, the variations of $\tilde{v}$ and $\tilde{\rho}$ with three different values of $\bar{m}$ are studied at a fixed supercooling, $S = 0.8$. The results are presented in Table II. Based on the data presented, we estimate that $\tilde{v} \sim \bar{m}^{1.1}$ and $\tilde{\rho} \sim \bar{m}^{-1.4}$. As we showed previously that the scaling of $\tilde{v}$ with S is rather insensitive to $\bar{m}$, it is reasonable to conjecture that $\tilde{v} \sim \bar{m}^{1.1}$ would hold for all S in the range studied.

We have plotted in Fig. 7 the variations of $\tilde{v}$ and $\tilde{\rho}$ with the fractional anisotropy of surface tension. It is evident that both the growth velocity and the tip radius vary as power laws of the strength of anisotropy, the former being an increasing function and the latter a decreasing function. According to a least squares fit, $\tilde{v} \sim \delta_\gamma^{0.84}$ and $\tilde{\rho} \sim \delta_\gamma^{-2.59}$ for $0.03 \leq \delta_\gamma \leq 0.05$.

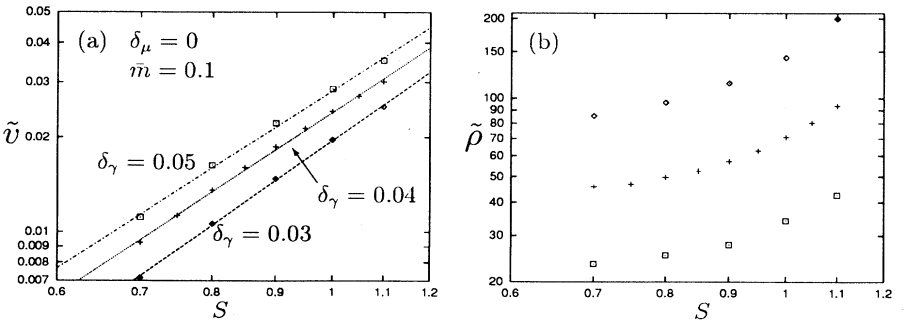

FIG. 5. Computed tip velocity $\tilde{v}$ and tip radius $\tilde{\rho}$ as a function of supercooling S (logarithmic scale) for two values of anisotropy. The straight lines through the values of the computed data points are least-squares fits. Diamonds are for $\delta_\gamma = 0.03$, crosses for $\delta_\gamma = 0.04$, and squares for $\delta_\gamma = 0.05$. The value of $\bar{m}$ is fixed at 0.1.

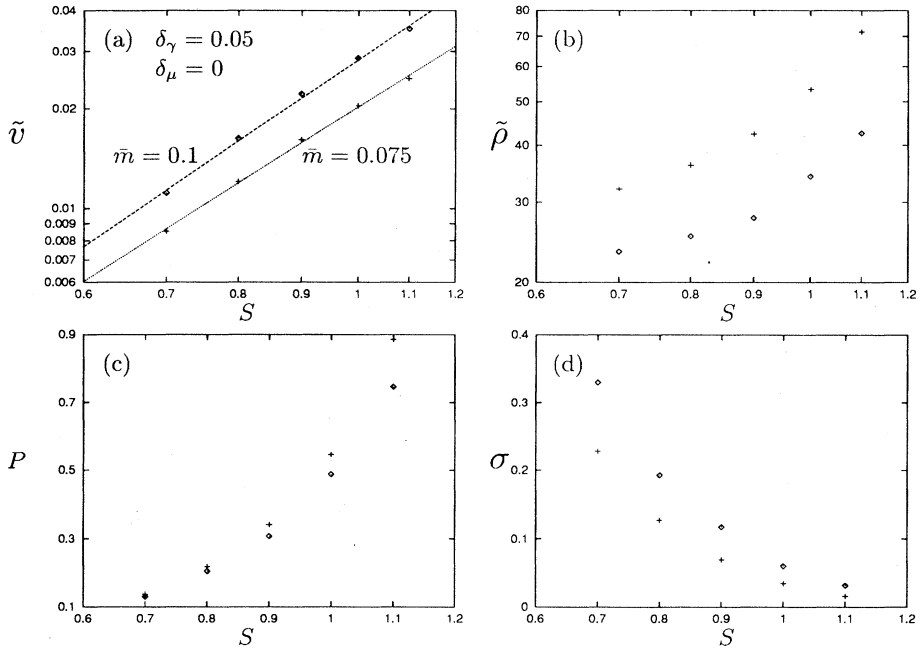

FIG. 6. Computed tip velocity $\tilde{v}$, tip radius $\tilde{\rho}$, corresponding Péclet number P, and selection parameter σ as a function of supercooling S for two values of $\bar{m}$. The straight lines through the values of the computed data points are least-squares fits. Diamonds are for $\bar{m} = 0.1$ and crosses for $\bar{m} = 0.075$. $\delta_\gamma = 0.05$ and $\delta_\mu = 0$. log-log scales are used in (a) and (b).

Since the growth velocity and the tip radius both increase with S, the Péclet number is an increasing function of S whereas σ is a decreasing function of S. The value of P is between 0.1 and 2.6 and σ is between 0.01 and 0.4 in the range of S where calculations were done. On the other hand, since the growth velocity and tip radius both exhibit scaling behavior with the strength of anisotropy, $P \sim \delta_\gamma^{-1.75}$ and $\sigma \sim \delta_\gamma^{4.34}$.

The plots in Figs. 6(c) and 6(d) display P and σ as a function of S for two different values of $\bar{m}$. As seen from the plots, a larger Péclet number and a smaller σ are associated with a smaller $\bar{m}$ for a fixed S.

A brief summary of case (i) follows.

(a) Power-law relationships between $\tilde{v}$ and $S, \bar{m}, \delta_\gamma$ are obtained. The exponents of S, $\bar{m}$, or δ_γ are somewhat insensitive to the values of the other two parameters. Therefore, we proceed to represent $\tilde{v}$ as a power-law function of S, $\bar{m}$, and δ_γ. An estimation of this function by a least-squares fit of the data obtained in this section yields

$$\tilde{v} \approx 3.55 \delta_\gamma^{0.78} \bar{m}^{1.08} S^{2.6}. \tag{18}$$

(b) The value of tip radius increases with S, but no power-law relationship is observed. $\tilde{\rho}$ decreases with $\bar{m}$ and δ_γ. For $S = 0.8$ and $\bar{m} = 0.1$, $\tilde{\rho} \sim \delta_\gamma^{-2.59}$.

(c) The Péclet number P increases with S and decreases with $\bar{m}$ and δ_γ.

(d) The selection parameter σ decreases with S, but increases with $\bar{m}$ and δ_γ.

B. Case (ii): Dendrites with $\delta_\gamma = 0$ and $\delta_\mu \neq 0$

We now proceed to discuss dendrites with anisotropic interface kinetics and isotropic surface tension [case (ii)]. The variation of $\tilde{v}$ with S is shown in Fig. 8(a) for $\bar{m} = 0.1$ and three different values of δ_μ. As in case (i), there is a power-law relationship between $\tilde{v}$ and S, as evident from the log-log plot. For a fixed S, the calculated value of $\tilde{v}$ increases with increasing δ_μ. The parameters of a least-squares fit for the computed data are shown in Table III. There is a 15% variation in the exponent of S as the value of δ_μ changes from 0.05 to 0.075. For $\bar{m} = 0.1$, a comparison of the best fit $\tilde{v} \sim S^{3.82}$ for $\delta_\mu = 0.05$

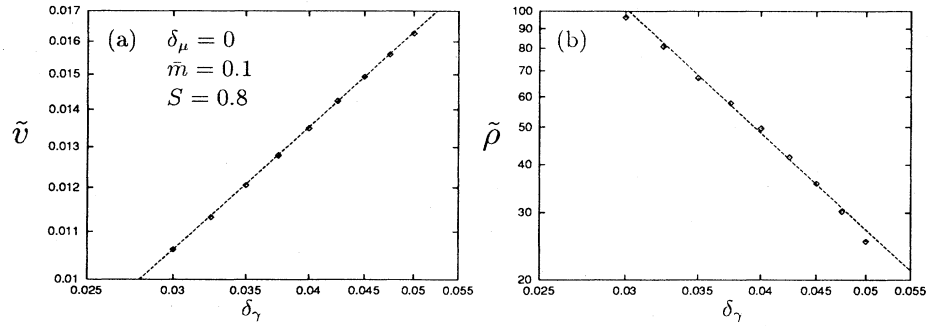

FIG. 7. Log-log plots of the tip velocity $\tilde{v}$ and tip radius $\tilde{\rho}$ as a function of the anisotropic surface tension δ_γ. The supercooling is fixed at $S = 0.8$. $\bar{m} = 0.1$ and $\delta_\mu = 0$. The straight lines through the values of the computed data points are least-squares fits.

TABLE II. Calculated tip velocity $\tilde{v}$ and tip radius $\tilde{\rho}$ for three different values of $\bar{m}$. The supercooling is fixed at $S = 0.8$.

δ_γ	δ_μ	$\bar{m}$	$\tilde{v}$	$\tilde{\rho}$
0.04	0	0.05	0.0061	134
0.04	0	0.075	0.0098	73
0.04	0	0.1	0.0135	50
0.05	0	0.05	0.0076	66
0.05	0	0.075	0.0120	36
0.05	0	0.1	0.0162	25

TABLE III. Least-squares fit of the growth velocity $\tilde{v}$ as a function of supercooling S, $\log \tilde{v} = a + b \log S$.

δ_γ	δ_μ	$\bar{m}$	a	b
0	0.05	0.1	-1.65	3.82
0	0.06	0.1	-1.60	3.64
0	0.075	0.1	-1.55	3.34
0	0.075	0.075	-1.66	3.10
0	0.075	0.05	-1.81	2.79

($\delta_\gamma = 0$) with that $\tilde{v} \sim S^{2.55}$ for $\delta_\gamma = 0.05$ ($\delta_\mu = 0$) in case (i) shows a difference of approximately 1.3 in the exponent of S.

The calculated values of $\tilde{v}$ as a function of S for $\delta_\mu = 0.075$ and three different values of $\bar{m}$ are presented in Fig. 9(a). Again, a linear dependence of $\log \tilde{v}$ on $\log S$ is evident from the log-log plot. The least-squares parameters are shown in Table III. An increase in $\tilde{v}$ is associated with increasing $\bar{m}$.

The dependence of $\tilde{\rho}$ on S with $\bar{m} = 0.1$ and three different values of δ_μ are presented in Fig. 8(b). Contrary to the *increasing* trend obtained in case (i), there is a definite *decrease* in $\tilde{\rho}$ with supercooling. As the values of the parameter δ_μ increase, $\tilde{\rho}$ decreases for a fixed S. For $\delta_\mu = 0.05$, the curve of $\tilde{\rho}$ versus S is somewhat "flattened" in the range $1.0 \leq S \leq 1.1$ as compared to the range $0.8 \leq S \leq 0.95$. A crude power-law approximation of $\tilde{\rho}$ versus S leads to $\tilde{\rho} \sim S^{-1.64}$ for $\delta_\mu = 0.075$, $\tilde{\rho} \sim S^{-1.51}$ for $\delta_\mu = 0.06$, and $\tilde{\rho} \sim S^{-1.32}$ for $\delta_\mu = 0.05$.

In Fig. 9(b) we plot the computed values of $\tilde{\rho}$ versus S for $\delta_\mu = 0.075$ and three different values of $\bar{m}$. As seen from the plot, there is a decreasing trend in $\tilde{\rho}$ with $\bar{m}$. A least-squares fit gives $\tilde{\rho} \sim S^{-1.22}$ for $\bar{m} = 0.05$, $\tilde{\rho} \sim S^{-1.42}$ for $\bar{m} = 0.075$, and, as obtained earlier, $\tilde{\rho} \sim S^{-1.64}$ for $\bar{m} = 0.1$.

Since $\tilde{v}$ is an increasing function of S and $\tilde{\rho}$ a decreasing function, the variations of P and σ with S need to be examined carefully. The values of P and σ corresponding to the computed values of $\tilde{v}$ and $\tilde{\rho}$ in Figs. 8(a) and 8(b) are presented in Fig. 8(c) and 8(d). The Péclet number is evidently an increasing function of supercooling and smaller values of P result from larger values of δ_μ. On the other hand, the value of σ is found to be small and weakly decreasing with supercooling. Note that for $\delta_\mu = 0.05$ and $\delta_\gamma = 0$, the value of σ is about 0.01 for $0.8 \leq S \leq 1.1$, whereas it ranges from 0.4 to 0.01 for $\delta_\gamma = 0.05$ and $\delta_\mu = 0$ in case (i).

We examined the effect of $\bar{m}$ on the values of P and σ for $\delta_\mu = 0.075$ in Figs. 9(c) and 9(d). We see that P increases with increasing $\bar{m}$, whereas σ has a weak dependence on S and it decreases slightly with increasing $\bar{m}$. Note that these behaviors are opposite those obtained in case (i).

Finally, we present the variation of $\tilde{v}$ and $\tilde{\rho}$ with δ_μ for $\bar{m} = 0.1$ and $S = 0.8$ in Fig. 10. Linear behaviors

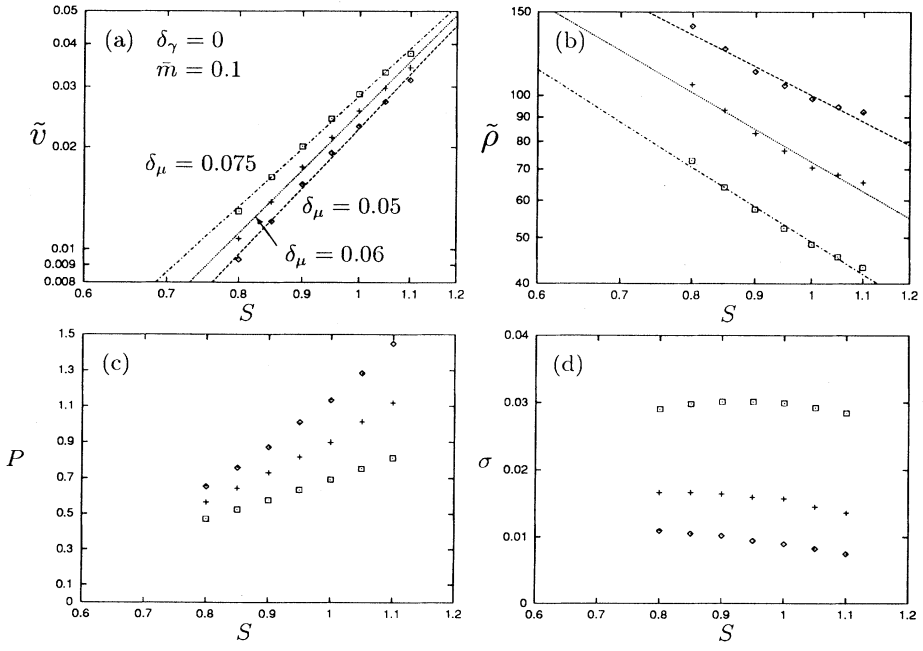

FIG. 8. Calculated values of the tip velocity $\tilde{v}$, tip radius $\tilde{\rho}$, Péclet number P, and selection parameter σ as a function of supercooling S for $\bar{m} = 0.1$ and $\delta_\gamma = 0$. Diamonds are for $\delta_\mu = 0.05$, crosses for $\delta_\mu = 0.06$, and squares for $\delta_\mu = 0.075$. The straight lines through the computed values of the data points are least-squares fits. log-log scales are used in (a) and (b).

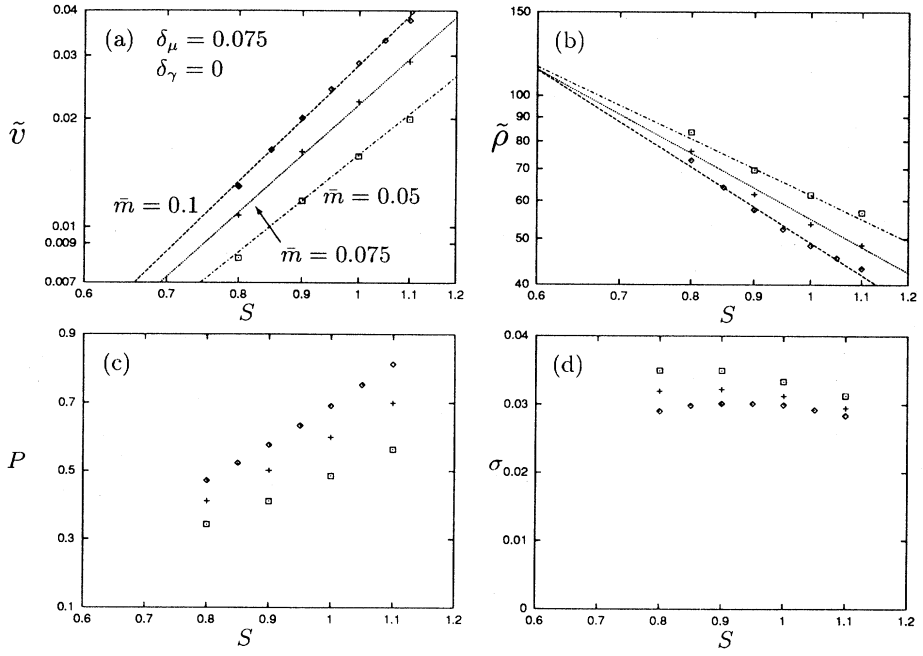

FIG. 9. Computed tip velocity $\tilde{v}$, tip radius $\tilde{\rho}$, Péclet number P, and selection parameter σ as a function of supercooling S for $\delta_\mu = 0.075$ and three values of $\bar{m}$. The straight lines through the values of the computed data points are least-squars fits. Diamonds are for $\bar{m} = 0.1$, crosses for $\bar{m} = 0.075$, and squares for $\bar{m} = 0.05$. $\delta_\mu = 0.075$ and $\delta_\gamma = 0$. log-log scales are used in (a) and (b).

are seen from the log-log plots. Least squares fits give $\tilde{v} \sim \delta_\mu^{0.82}$ and $\tilde{\rho} \sim \delta_\mu^{-1.62}$. Correspondingly, $P \sim \delta_\mu^{-0.80}$ and $\sigma \sim \delta_\mu^{2.42}$.

The results of this subsection may be summarized as follows.

(a) As in case (i), a power-law relationship is observed between $\tilde{v}$ with each of the parameters $S, \bar{m}, \delta_\mu$. A least-squares fit of the data obtained in this section leads to

$$\tilde{v} \approx 0.96\delta_\mu^{0.64}\bar{m}^{0.81}S^{3.5}. \tag{19}$$

(b) The tip radius is a decreasing function of S, δ_μ, and $\bar{m}$.

(c) The Péclet number is found to be an increasing function of S and $\bar{m}$. However, its value decreases with δ_μ.

(d) The selection parameter σ decreases somewhat with S, although the calculated values depend weakly on S. Its value is *larger* for *smaller* $\bar{m}$ and larger δ_μ.

C. Case (iii): Dendrites with $\delta_\gamma \neq 0$ and $\delta_\mu \neq 0$

In this section, we study dendrites with anisotropic surface tension and interface kinetics [case (iii)]. As will become apparent later, the relative strengths of the anisotropies alter the functional dependence of the Péclet number on $\bar{m}$. We first discuss cases where $\delta_\gamma = \delta_\mu$, followed by cases in which $\delta_\gamma \neq \delta_\mu$.

1. $\delta_\gamma = \delta_\mu \neq 0$

The variations of the growth velocity with supercooling are studied for $\delta_\gamma = \delta_\mu = 0.03$ and 0.04, respectively, and three values of $\bar{m} = 0.05, 0.075, 0.1$. The results are shown in Figs. 11(a) and 12(a).

The following observations may be made from the plots.

(a) Among the three values of $\bar{m}$ studied, for each fixed

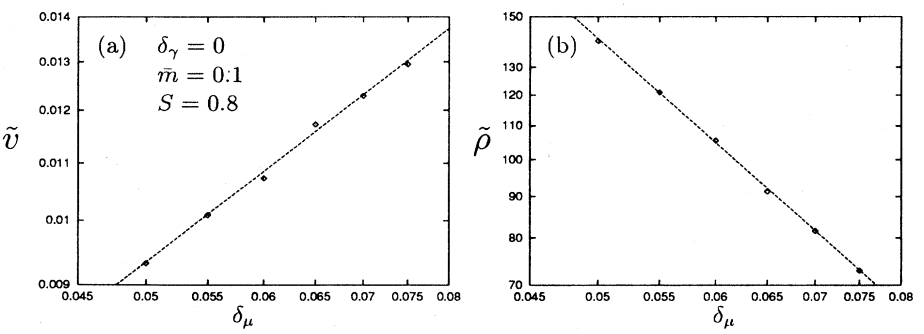

FIG. 10. Log-log plots of the tip velocity $\tilde{v}$ and the tip radius $\tilde{\rho}$ as a function of δ_μ. The other parametes are fixed: $S = 0.8$, $\bar{m} = 0.1$, and $\delta_\gamma = 0$. The straight lines through the values of the computed data points are least-squares fits.

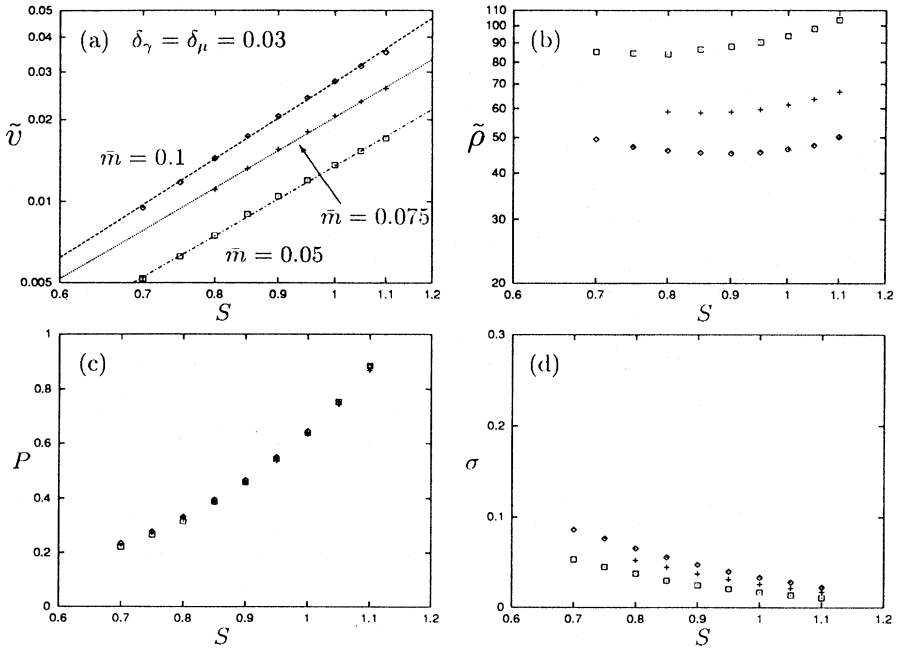

FIG. 11. Computed tip velocity $\tilde{v}$ and tip radius $\tilde{\rho}$ as a function of supercooling S for $\delta_\gamma = \delta_\mu = 0.03$ and three values of $\bar{m}$. The straight lines through the values of the computed data points are least-squares fits. Diamonds are for $\bar{m} = 0.1$, crosses for $\bar{m} = 0.075$, and squares for $\bar{m} = 0.05$. log-log scales are used in (a) and (b).

anisotropy, $\bar{m} = 0.1$ gives the largest value of $\tilde{v}$, followed by $\bar{m} = 0.075$ and then $\bar{m} = 0.05$.

(b) Anisotropy of $\delta_\gamma = \delta_\mu = 0.04$ leads to larger $\tilde{v}$ than anisotropy of $\delta_\gamma = \delta_\mu = 0.03$ for a fixed S.

(c) The relationship between $\log \tilde{v}$ and $\log S$ is linear. The parameters from least squares fits are given in Table IV. There is about a 10% variation in the exponent of S when $\bar{m}$ decreases from 0.1 to 0.05 for each fixed value of $\delta_\gamma = \delta_\mu$.

Shown in Figs. 11(b) and 12(b) are the calculated values of the tip radius as a function of S for various values of δ_γ and $\bar{m}$. Interestingly, when the strengths of anisotropies are the same, the value of $\tilde{\rho}$ decreases with S for lower values of S but increases with S for higher values of S. This "swing" behavior seems to be a "mixture" of those in cases (i) and (ii). Roughly speaking, the values of $\tilde{\rho}$ do not change significantly with S. We notice that the swing behaviors are not sensitive to the

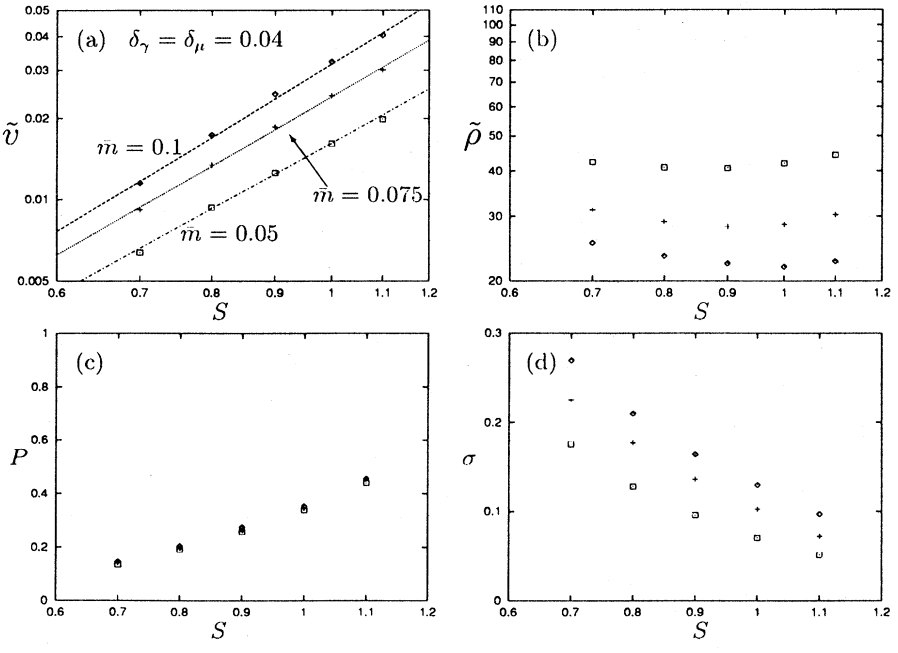

FIG. 12. Computed tip velocity $\tilde{v}$ and tip radius $\tilde{\rho}$ as a function of supercooling S for $\delta_\gamma = \delta_\mu = 0.04$ and three values of $\bar{m}$. The straight lines through the values of the computed data points are least-squares fits. Diamonds are for $\bar{m} = 0.1$, crosses for $\bar{m} = 0.075$, and squares for $\bar{m} = 0.05$. log-log scales are used in (a) and (b).

TABLE IV. Least-squares fit of the growth velocity $\tilde{v}$ as a function of supercooling S, $\log \tilde{v} = a + b \log S$.

δ_γ	δ_μ	$\bar{m}$	a	b
0.03	0.03	0.1	-1.56	2.93
0.03	0.03	0.075	-1.69	2.69
0.03	0.03	0.05	-1.87	2.65
0.04	0.04	0.1	-1.50	2.79
0.04	0.04	0.075	-1.62	2.64
0.04	0.04	0.05	-1.80	2.52

TABLE V. Calculated tip velocity $\tilde{v}$ and tip radius $\tilde{\rho}$ and the corresponding Péclet number P for various values of $\bar{m}$.

δ_γ	δ_μ	S	$\bar{m}$	$\tilde{v}$	$\tilde{\rho}$	P
0.03	0.03	0.8	0.025	0.0039	167	0.326
0.03	0.03	0.8	0.05	0.0075	84	0.315
0.03	0.03	0.8	0.075	0.0111	59	0.327
0.03	0.03	0.8	0.1	0.0144	46	0.331
0.03	0.03	0.9	0.025	0.0052	179	0.465
0.03	0.03	0.9	0.05	0.0105	88	0.462
0.03	0.03	0.9	0.075	0.0156	59	0.460
0.03	0.03	0.9	0.1	0.0206	45	0.463

fact that we used a hyperbola to calculate the tip radius. Calculation of the tip radius by fitting the interface to a parabola (see Sec. III) also display the swing trend. An increase of $\tilde{\rho}$ is associated with decreasing $\bar{m}$ and increasing anisotropy.

The Péclet number P and the selection parameter σ corresponding to the calculated values of $\tilde{v}$ and $\tilde{\rho}$ in Figs. 11(a), 11(b), Fig. 12(a), and 12(b) are shown in Figs. 11(c), 11(d), Fig. 12(c), 12(d). From the plots, we can make the following observations.

(a) Since $\tilde{v}$ increases as S whereas $\tilde{\rho}$ has a weak functional dependence on S, P is an increasing function and σ is a decreasing function of S.

(b) For the same anisotropy and supercooling, the value of P is almost identical for the three values of $\bar{m}$ studied. Computations repeated with finer resolution, i.e., $\bar{\epsilon} = \delta x = 1/800$, also show the same behaviors.

(c) Smaller anisotropy leads to a larger value of P.

(d) The selection parameter $\sigma = 2/(\tilde{v}\tilde{\rho}^2) = \tilde{v}/(2P^2)$ has the same functional dependence on $\bar{m}$ as $\tilde{v}$, that is, the value of σ increases with increasing $\bar{m}$.

(e) The value of σ increases with anisotropy in the range $0.03 \leq \delta_\gamma \leq 0.04$.

Observation (b) suggests that P might be independent of $\bar{m}$. To test this suspicion, we performed two computations with $\bar{m} = 0.025$, $S = 0.8$ and $\bar{m} = 0.025$, $S = 0.9$. The results are presented in Table V, along with the results for other values of $\bar{m}$ studied previously. The value of P is seen to be insensitive to $\bar{m}$ with an even stronger interface kinetic effect ($\bar{m} = 0.025$). A least-squares fit leads to $\tilde{v} \sim \bar{m}^{0.95}$, and $\tilde{\rho} \sim \bar{m}^{-0.93}$ for $S = 0.8$ and $\tilde{v} \sim \bar{m}^{0.99}$ and $\tilde{\rho} \sim \bar{m}^{-1}$ for $S = 0.9$.

The calculated values of $\tilde{v}$ and $\tilde{\rho}$ as a function of $\delta_\gamma = \delta_\mu$ for $\bar{m} = 0.1$ and $S = 0.8$ are shown in Fig. 13. An increase of the anisotropy increases the velocity and decreases the tip radius. Linear relationships are obvious on the log-log plots that yield $\tilde{v} \sim \delta_\gamma^{0.69}$, and $\tilde{\rho} \sim \delta_\gamma^{-2.26}$. Consequently, $P \sim \delta_\gamma^{-1.57}$ and $\sigma \sim \delta_\gamma^{3.83}$.

A brief summary of this subsection is as follows.

(a) As in previous cases, $\tilde{v}$ is found to have power-law relationships with S, $\bar{m}$, and δ_γ. A best fit gives

$$\tilde{v} \approx 2.12 \delta_\gamma^{0.61} \bar{m}^{0.96} S^{2.7}. \tag{20}$$

(b) The value of $\tilde{\rho}$ is weakly dependent on S with a swing trend between cases (i) and (ii). Its value decreases with $\bar{m}$ and δ_γ.

(c) P is *insensitive* to $\bar{m}$ for fixed S and anisotropy.

(d) σ decreases with S but *increases* with $\bar{m}$ and anisotropy.

2. $\delta_\gamma \neq \delta_\mu \neq 0$

Behaviors of dendrites with $\delta_\gamma \neq \delta_\mu \neq 0$ are studied in this subsection. For ease of presentation, we subdivide these into two categories: (i) $\delta_\gamma > \delta_\mu$ and (ii) $\delta_\gamma < \delta_\mu$.

First, we discuss the calculated operating state of dendrites with $\delta_\gamma = 0.04$ and $\delta_\mu = 0.02$ ($\delta_\gamma > \delta_\mu$). The calculated values of $\tilde{v}$ as a function of S for three values of $\bar{m}$ are shown in Fig. 14(a). Again, linear behaviors are evident in the log-log plot. The parameters of least-

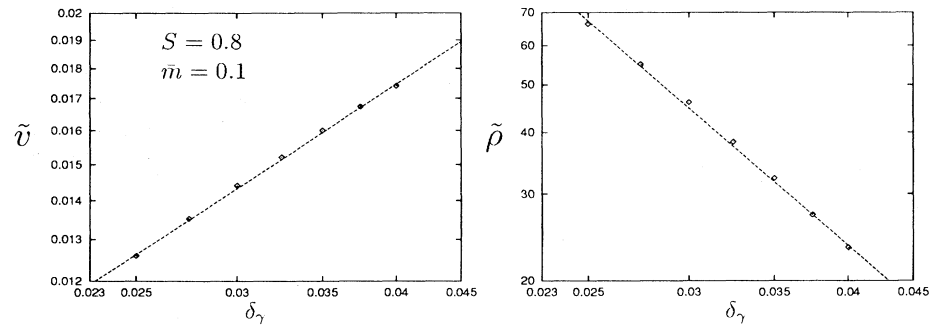

FIG. 13. Log-log plots of the calculated tip velocity $\tilde{v}$ and tip radius $\tilde{\rho}$ as a function of $\delta_\gamma = \delta_\mu$. The other parameters at $S = 0.8$ and $\bar{m} = 0.1$. The straight lines through the values of the computed data points are least-squares fits.

TABLE VI. Least-squares fit of the growth velocity $\tilde{v}$ as a function of supercooling S, $\log \tilde{v} = a + b \log S$.

δ_γ	δ_μ	$\bar{m}$	a	b
0.04	0.02	0.1	-1.54	2.75
0.04	0.02	0.075	-1.68	2.61
0.04	0.02	0.05	-1.86	2.47
0.03	0.04	0.1	-1.53	2.96
0.03	0.04	0.075	-1.66	2.77
0.03	0.04	0.05	-1.83	2.64

squares fits are tabulated in Table VI. The exponents of S vary by about 10% as the value of $\bar{m}$ changes from 0.1 to 0.05. Note that, for the same $\bar{m}$, the exponents of S are almost equal to those with $\delta_\gamma = \delta_\mu = 0.04$, as listed in Table V.

For a fixed S, a larger $\tilde{v}$ is obtained with $\bar{m} = 0.1$, followed by $\bar{m} = 0.075$ and then $\bar{m} = 0.05$. We note that, for each $\bar{m}$ and S, the calculated value of $\tilde{v}$ shown in this plot is smaller than that in Fig. 12(a), where $\delta_\gamma = \delta_\mu = 0.04$. To study further whether the value of $\tilde{v}$ is increased by an increase in anisotropy, we proceed to examine $\tilde{v}$ for different values of δ_γ and δ_μ for $S = 0.8$ and $\bar{m} = 0.1$. As shown in Fig. 15(a), for a fixed δ_γ, $\tilde{v}$ increases as δ_γ increases from 0 to 0.04 and, for a fixed δ_μ, $\tilde{v}$ is increased when δ_γ increases from 0.03 to 0.04. Therefore, $\tilde{v}$ is increased by an increase in either δ_γ or δ_μ.

The variation of $\tilde{\rho}$ with S for three values of $\bar{m}$ is shown in Fig. 14(b). No power-law relationship could be discerned from the log-log plot. For a fixed $\bar{m}$, the value of $\tilde{\rho}$ increases somewhat with S. We note that the increasing rate for the curve of $\tilde{v}$ versus S for $\bar{m} = 0.1$ is less than that for $\delta_\gamma = 0.04$ and $\delta_\mu = 0$, plotted in Fig. 5. Also recall that the variation of $\tilde{v}$ with S displayed a swing behavior for $\delta_\gamma = \delta_\mu = 0.04$, shown in Fig. 12. Therefore, with $\delta_\gamma = 0.04$, the functional dependence of $\tilde{\rho}$ on S is seen to be influenced by the value of δ_μ ranging from 0 to 0.02 to 0.04.

For a fixed S, $\tilde{\rho}$ decreases with $\bar{m}$. For each S and $\bar{m}$, the calculated value of $\tilde{\rho}$ is smaller than that for $\delta_\gamma = \delta_\mu = 0.04$. For $\bar{m} = 0.1$ and $S = 0.8$, the value of $\tilde{\rho}$ decreases either with δ_μ and fixed δ_γ, or as δ_γ changes from 0.03 to 0.04 and various fixed values of δ_μ.

As both $\tilde{v}$ and $\tilde{\rho}$ increase with S, P is increased and σ is decreased with increasing S, as shown in Figs. 14(c) and 14(d). For smaller values of S ($0.7 \leq S \leq 0.9$), the value of P is almost identical for the values of $\bar{m}$ studied. For larger values of S, for instance for $S = 1.1$, the value of P decreases as $\bar{m}$ increases from 0.05 to 0.1, similar to case (i). The value of σ is increased with $\bar{m}$. As shown in Figs. 15(c) and 15(d), an increase in δ_μ in the range $0 \leq \delta_\mu \leq 0.04$ brings about a decrease in P and an increase in σ for $S = 0.8$, $\bar{m} = 0.1$, and $\delta_\gamma = 0.03$ or 0.04.

Finally, we discuss the results for $\delta_\gamma = 0.03$ and $\delta_\mu = 0.04$ ($\delta_\gamma < \delta_\mu$). The variation of $\tilde{v}$ with S for various values of $\bar{m}$ shown in Fig. 16. From Fig. 16(a), it is evident that $\log \tilde{v}$ is linearly dependent on $\log S$. The parameters for least-squares fits are tabulated in Table VI. There is a 10% variation in the exponent of S as $\bar{m}$ decreases from 0.1 to 0.05. Again, for fixed S, the value of $\tilde{v}$ increases with $\bar{m}$. It is instructive to compare the plot with Fig. 12(a), which is for $\delta_\gamma = \delta_\mu = 0.04$. We see that, for fixed S and $\bar{m}$, the calculated values of $\tilde{v}$ are smaller for $\delta_\gamma = 0.03$ and $\delta_\mu = 0.04$ than for $\delta_\gamma = \delta_\mu = 0.04$. In other words, with the presence of interface kinetic anisotropy $\delta_\mu = 0.04$, an increase in δ_γ from 0.03 to 0.04 causes an increase in $\tilde{v}$.

The calculated values of $\tilde{\rho}$ as a function of S are shown in Fig. 16(b). Unlike the increasing trend for $\delta_\gamma = 0.04$

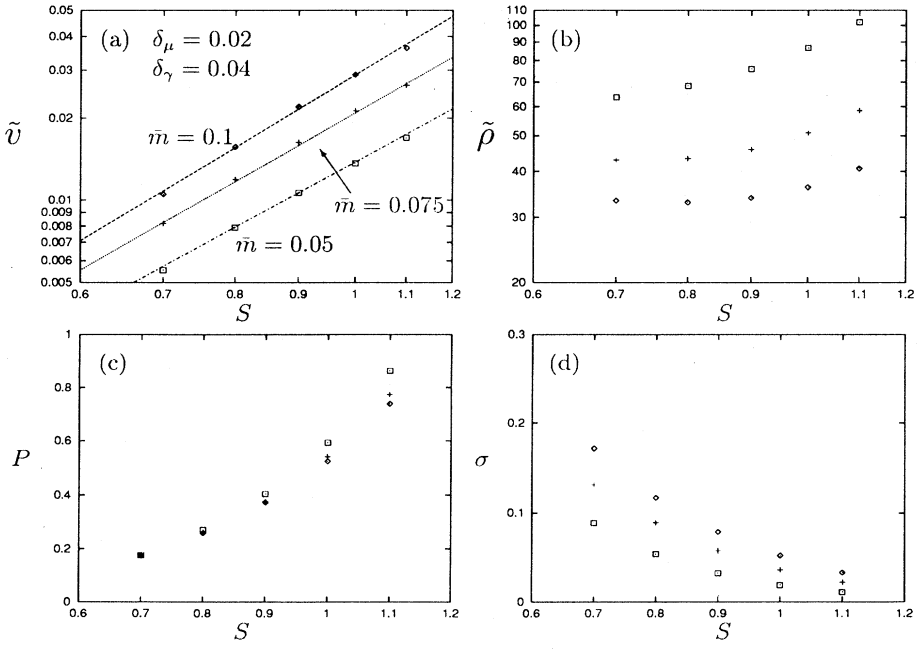

FIG. 14. Calculated values of the tip velocity $\tilde{v}$, tip radius $\tilde{\rho}$, and corresponding P and σ as a function of supercooling S for $\delta_\gamma = 0.04$ and $\delta_\mu = 0.02$. Diamonds are for $\bar{m} = 0.1$, crosses for $\bar{m} = 0.075$, and squares for $\bar{m} = 0.05$. Log-log scales are adopted in (a) and (b).

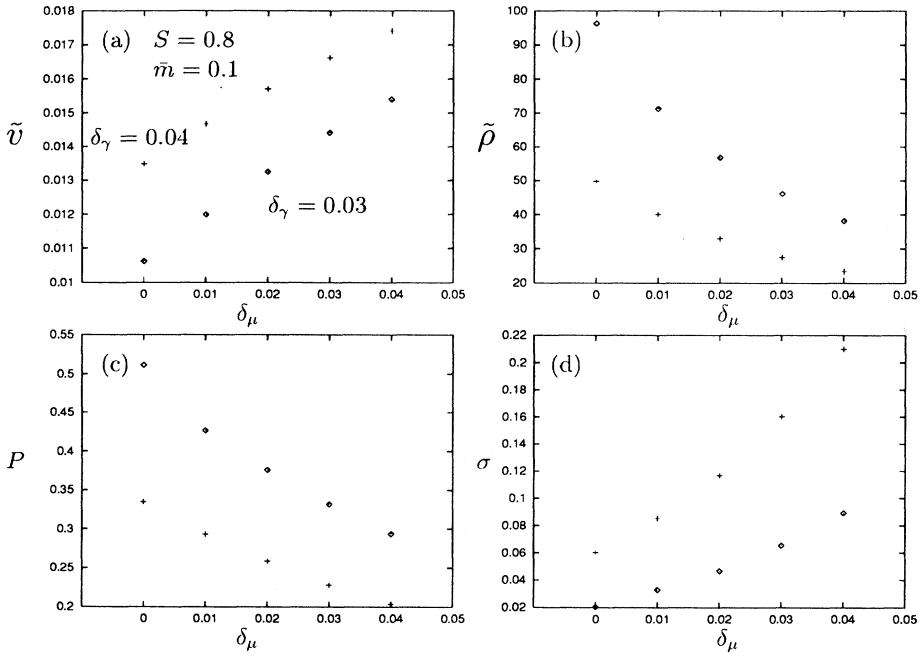

FIG. 15. Calculated values of $\tilde{v}$, $\tilde{\rho}$, and corresponding P and σ as a function of δ_μ with two nonzero values of δ_γ. Diamonds are for $\delta_\gamma = 0.03$ and crosses for $\delta_\gamma = 0.04$. The value of S is fixed at 0.8 and $\bar{m} = 0.1$.

and $\delta_\mu = 0.02$ ($\delta_\gamma > \delta_\mu$), $\tilde{\rho}$ was seen to decrease with S for $0.7 \leq S \leq 0.9$ and change rather slowly with S for higher values of S. This behavior is similar to the swing behavior observed in Sec. IV C 1, where $\delta_\gamma = \delta_\mu$. Note that for each fixed S and $\bar{m}$, the calculated values of $\tilde{\rho}$ are smaller than those in Fig. 14(b).

Since $\tilde{v}$ increases with S whereas $\tilde{\rho}$ depends weakly on S, P is increased and σ is decreased with S. For smaller values of S ($0.7 \leq S \leq 0.9$), P is found to be almost identical for the values of $\bar{m}$ studied. For larger values of S, however, P is somewhat decreased with $\bar{m}$, as shown in Fig. 16. This trend is opposite to that for dendrites with $\delta_\gamma = 0.04$ and $\delta_\mu = 0.02$ ($\delta_\gamma > \delta_\mu$). On the other hand, the values of σ are increased with $\bar{m}$, as in case (i) and as in cases with $\delta_\gamma = 0.04$ and $\delta_\mu = 0.02$ ($\delta_\gamma > \delta_\mu$).

The observations in this subsection are summarized below.

(a) As in the previous cases, $\tilde{v}$ increases with $\bar{m}$ and a power-law relationship exists between $\tilde{v}$ and S. For

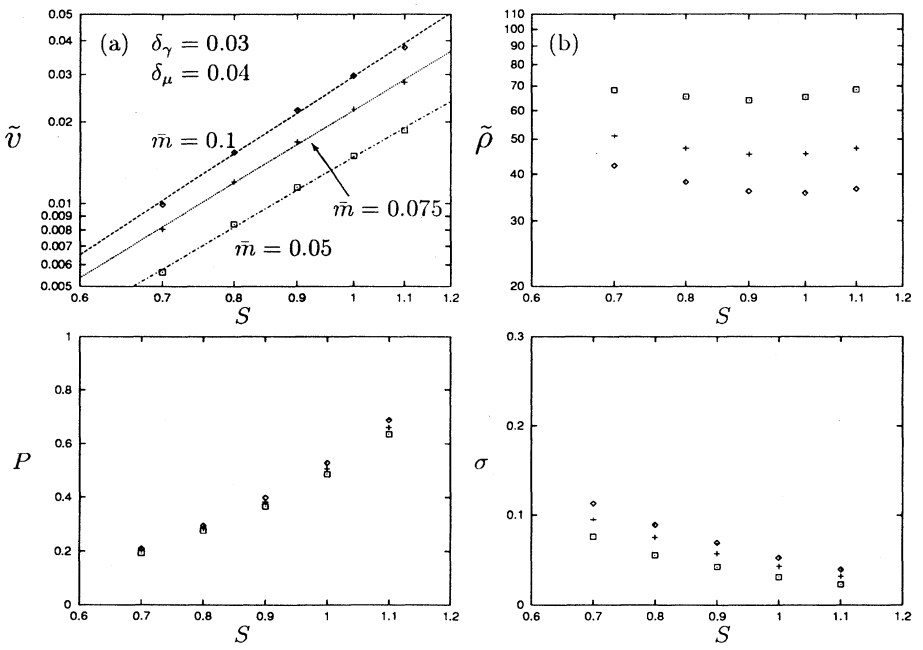

FIG. 16. Calculated values of the tip velocity $\tilde{v}$ and tip radius $\tilde{\rho}$ as a function of supercooling S for $\delta_\gamma = 0.03$ and $\delta_\mu = 0.04$. Diamonds are for $\bar{m} = 0.1$, crosses for $\bar{m} = 0.075$, and squares for $\bar{m} = 0.05$. Log-log scales are used in (a) and (b).

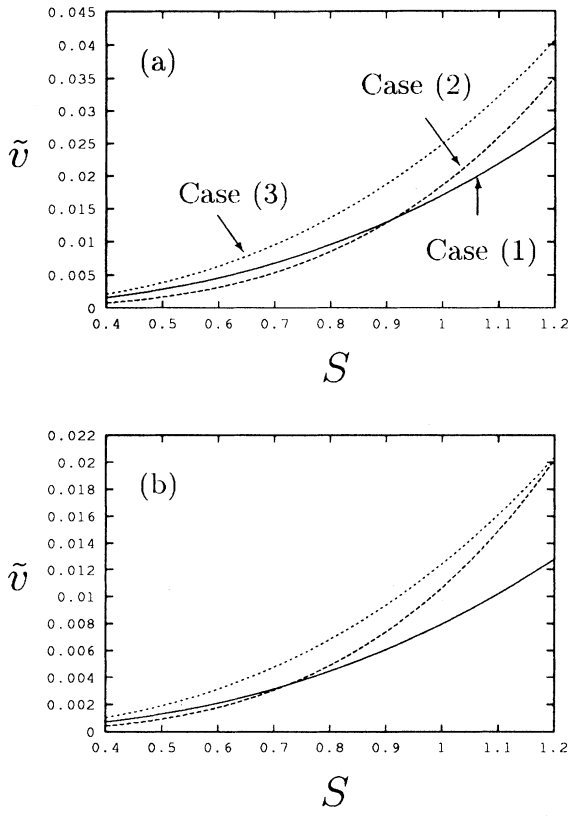

FIG. 17. Estimated values of $\tilde{v}$ as a function of S. The full line is for $\delta_\gamma = 0.03$ and $\delta_\mu = 0$ [case (i)]; the dashed line for $\delta_\gamma = 0$ and $\delta_\mu = 0.03$ [case (ii)], and the dotted line for $\delta_\gamma = \delta_\mu = 0.03$ [case (iii)]. The value of $\bar{m}$ is 0.1 in (a) and 0.05 in (b).

various values of $\bar{m}$, the exponent of S does not change substantially with each fixed anisotropy. As in previous cases, a least-squares fit of the data obtained in this subsection, along with those in Sec. IV C 1 ($\delta_\gamma = \delta_\mu$), leads to

$$\tilde{v} \approx 2.04\delta_\gamma^{0.41}\delta_\mu^{0.19}\bar{m}^{0.97}S^{2.7}. \tag{21}$$

(b) The value of $\tilde{\rho}$ increases with S for dendrites with $\delta_\gamma > \delta_\mu$. For dendrites with $\delta_\gamma < \delta_\mu$, $\tilde{\rho}$ again displays the swing behavior, observed for dendrites with $\delta_\gamma > \delta_\mu$. For a fixed S and a fixed anisotropy, $\tilde{\rho}$ decreases with $\bar{m}$. For $S = 0.8$ and $\bar{m} = 0.1$, $\tilde{\rho}$ decreases either with δ_μ ranging from 0 to 0.04 and a fixed value of δ_γ, or with δ_γ increasing from 0.03 to 0.04 and a fixed value of δ_μ.

(c) P increases with S and decreases with increasing anisotropy. Among the three values of $\bar{m}$ studied, P was almost identical for $0.7 \leq S \leq 0.9$. For $1.0 \leq S \leq 1.1$, P decreases somewhat with $\bar{m}$ for dendrites with $\delta_\gamma > \delta_\mu$ and increases for dendrites with $\delta_\gamma < \delta_\mu$. The former is similar to case (i) and the latter to case (ii).

(d) σ decreases with S, $\bar{m}$, and anisotropy.

V. DISCUSSION

Much work on dendritic growth, both analytic and numerical, has been devoted to the determination of the selection parameter σ, based on WKB analysis, in which the Péclet number P has been considered as a parameter determined according to the Ivantsov relation. This Ivantsov relation pertains to a parabola that represents the *asymptotic shape* of a branchless needle crystal far from the tip. The operating state is then calculated by combining σ and P. In other words, this P, which relates to ρ_a, the tip radius of the asymptotic parabola, is determined solely by the supercooling while the anisotropies of surface tension and interface kinetics are shown to play crucial roles in determining σ.

In contrast, we obtained the growth velocity and actual tip radius of dendrites explicitly as functions of S, $\bar{m}$, δ_γ, and δ_μ. The reliability of these results is bolstered by the fact that the computed tip temperatures are observed to be in very good agreement with the asymptotic result

$$u = -\frac{1}{S\left\{L_0/(cT_M) + \left([1 - 15\delta_\gamma\cos(4\theta)]\frac{1}{\tilde{\rho}} + \frac{\tilde{v}/\bar{m}}{[1+\delta_\mu\cos(4\theta)]}\right)^{-1}\right\}}, \tag{22}$$

which is derived from Eq. (72) in [47] without linearizing $\tilde{Q}(u)$. Instead, we use $\tilde{Q}(u) = u/(1+u)$, which follows from Eq. (39) in [47] for constant $\tilde{L}$. This nonlinear equation is in agreement with the nonlinear Gibbs-Thomson equation derived by Gurtin [61] in the absence of anisotropies and kinetics.

Our numerical data have shown that the functional dependence of P on $\bar{m}$ is strongly influenced by anisotropies. In case (i), where $\delta_\gamma \neq 0$ and $\delta_\mu = 0$, P is seen to decrease with $\bar{m}$; in case (ii), where $\delta_\gamma = 0$ and $\delta_\mu \neq 0$, P increases with $\bar{m}$. When $\delta_\gamma = \delta_\mu$, P is almost independent of $\bar{m}$. At large supercoolings $S \geq 1$, P decreases slightly with $\bar{m}$ for $\delta_\gamma > \delta_\mu \neq 0$ and increases slightly for $\delta_\mu > \delta_\gamma \neq 0$. As P is found to increase with S in each case, it decreases with either δ_γ or δ_μ. Therefore, the value of P is not only dependent on S, but also on $\bar{m}$ and the anisotropies δ_γ and δ_μ.

The calculated values of $\tilde{v}$ were found to increase as power laws of S, $\bar{m}$, and anisotropies. The exponents of either S, $\bar{m}$, δ_γ, or δ_μ are slightly dependent on the values of the other three parameters. In particular, the exponent of S decreases monotonically with $\bar{m}$ decreasing from 0.1 to 0.05. Combining all the calculated results in each case, the velocity obtained by least-squares fits has the form

$$\tilde{v} \approx \begin{cases} 3.55\delta_\gamma^{0.78}\bar{m}^{1.08}S^{2.6}, & 0.03 \le \delta_\gamma \le 0.05, \quad \delta_\mu = 0, & 0.7 \le S \le 1.1 \\ 0.96\delta_\mu^{0.64}\bar{m}^{0.81}S^{3.5}, & \delta_\gamma = 0, & 0.05 \le \delta_\mu \le 0.075, \quad 0.8 \le S \le 1.1 \\ 2.04\delta_\gamma^{0.41}\delta_\mu^{0.19}\bar{m}^{0.97}S^{2.7}, & 0.03 \le \delta_\gamma \le 0.04, & 0.01 \le \delta_\mu \le 0.04, \quad 0.7 \le S \le 1.1, \end{cases}$$

with the value of $\bar{m}$ ranging from 0.05 to 0.1. These summary results are useful to compare overall trends but are not, of course, an accurate substitute for the specific results presented earlier.

The exponent of S in case (ii) is larger by approximately 1 than in case (i) and the exponent in case (iii) is about equal to that in case (i). It was noted in [62], in which the boundary layer model was studied with sixfold sinusoidal anisotropy at the interface, that, for $0.2 < S < 0.6$, $\tilde{v} \sim S^5$ in case (i) while $\tilde{v} \sim S^8$ in case (ii). Therefore, a rough difference in the exponent of approximately 3 is evident. When both anisotropies were taken into account simultaneously, these authors did not find a power-law relationship.

Based on nonlocal solvability theory, Brener [7] obtained analytically the growth rate as a function of Péclet number at the limit of low Péclet number and small anisotropy. He found that $\tilde{v} \sim P^{1/6}$ for case (i) and $\tilde{v} \sim P^{11/2}$ for case (ii). Since at lower Péclet number $P \approx S^2$ according to the Ivantsov relation, this would mean that $\tilde{v} \sim S^{1/3}$ and $\tilde{\rho} \sim S^{5/3}$ in case (i) and $\tilde{v} \sim S^{11}$ and $\tilde{\rho} \sim S^{-9}$ in case (ii). Thus the difference in the exponents (≈ 11) of S is rather large. Brener concluded that, when both anisotropies are considered simultaneously, an increase in either anisotropy results in an increase in $\tilde{v}$. However, he did not provide an explicit functional dependence of $\tilde{v}$ on P. It is worth stressing the fact that the ranges of S over which conclusions were made in the studies cited above do not overlap at all with ours.

We note that, although the exponent of $\bar{m}$ is slightly different in each of cases (i), (ii), and (iii), its value is approximately one, i.e., $\tilde{v} \propto \bar{m}$. Thus, in terms of dimensional quantities, we have $v = \tilde{v}(\kappa/d_0)$, i.e.,

$$v \propto \frac{\bar{m}\kappa}{d_0} = \frac{\kappa}{\rho_K} = \frac{\bar{\mu}L_0}{c},$$

independent of the strength of surface tension $\bar{\gamma}$ and thermal diffusivity, although it depends on the *anisotropy* of the surface tension through δ_γ. Apparently, such dendrites behave as "kinetic dendrites" with ρ_K being the significant length.

We emphasize the fact that the ranges of δ_γ and δ_μ in the three cases we studied do not overlap. To compare quantitatively the growth velocity of dendrites in the three cases, we examine the possibility that extrapolation of $\tilde{v}$ is possible for the values of parameters S, $\bar{m}$, δ_γ, and δ_μ outside the range used in our computations. In Fig. 17(a) we plot the estimated values of $\tilde{v}$ as a function of S with the same strength of anisotropy ($\delta_\gamma = 0.03$ and $\delta_\mu = 0.03$) and interface kinetics ($\bar{m} = 0.1$) in all three cases. Apparently, the value of $\tilde{v}$ associated with both anisotropies [case (3)] is shifted to be larger than that with either anisotropy [cases (i) and (ii)]. At lower values of S, $\tilde{v}$ in case (iii) is closer to that in case (i) whereas at larger values of S, $\tilde{v}$ is closer to that in case (ii). Thus, in systems with the same strength of surface tension and interface kinetics, the surface tension anisotropy dominates the growth of the dendrite at small supercoolings, whereas at large supercoolings the interface kinetic anisotropy becomes more dominant. Similar conclusions were drawn in the two studies cited earlier [7,62]. With stronger interface kinetics (smaller value of $\bar{m} = 0.05$), the domination of the kinetic anisotropy is more significant, as shown in Fig. 17(b). Note that the "turning point," S_c at which the value of $\tilde{v}$ in case (ii) equals that in case (i) with the same strength of anisotropy may be given by

$$S_c \sim \delta_\gamma^{0.2}\bar{m}^{0.3},$$

i.e., S_c increases with $\bar{m}$ and δ_γ.

We proceed to make another extrapolation of $\tilde{v}$ for $\bar{m} = 0.025$ and $\delta_\gamma = \delta_\mu = 0.03$ in case (iii). By using the material parameters for nickel listed in [53], dimensional velocities in the range of 40–80 m/sec are obtained for supercooling temperatures between 240 and 320 K. Note that the chosen value of $\bar{m} = 0.025$ corresponds to a kinetic coefficient $\mu = 140$ cm/sec, which is the same value derived from a collision-limited growth model [63]. The values of our estimated growth velocity are found to fall in the range of experimental values measured by Willnecker *et al.* [22]. Unfortunately, a more detailed comparison with the experimental data is not quite practical as the anisotropy of surface tension and interface kinetics of nickel is still not available. On the other hand, for an anisotropy three times larger or smaller, the growth velocity is estimated to increase or decrease by 2. Therefore, the extrapolation of our two-dimensional numerical results for $\bar{m} = 0.025$, $0.01 \le \delta_\gamma = \delta_\mu \le 0.09$, and $0.6 \le S \le 0.8$ give growth velocities of nickel dendrites of the same order as three dimensional experimental data.

The functional dependence of $\tilde{\rho}$ on S is different in each case: $\tilde{\rho}$ is found to increase with S in case (i), decrease in case (ii), and to behave as a mixture of these previous two cases in case (iii). Therefore, the surface tension anisotropy and the interface kinetic anisotropy seem to play different roles in determining the tip radius, contrary to their role in determining tip velocity. We did not observe a power-law relationship between $\tilde{\rho}$ and S in cases (i) and (iii). In case (ii) a rough power-law behavior is observed; a crude approximation gives $\tilde{\rho} \sim S^{-1.5}$. As mentioned earlier, in the limit of small Péclet number, $\tilde{\rho} \sim S^{5/3}$ for case (i) and $\tilde{\rho} \sim S^{-9}$ for case (ii) would be obtained by Brener [7]. Thus he would expect that $\tilde{\rho}$ increases with S for case (i) and decreases with S in case (ii), similar to our results. However, his rate of increase or decrease is very different from ours.

The value of σ decreases with S in cases (i) and (iii). In case (ii) its value is hardly changed with S, although a decreasing trend may be detected. Thus σ is a decreasing function of S in models that include the interface kinet-

ics effect (nonzero value of $\bar{m}$) and either anisotropy of surface tension and interface kinetics. Recently, Sekerka [12] made an *optimal stability* conjecture that allows interface kinetics to be considered in the determination of the dendritic operating states. His model leads to the prediction that σ is a decreasing function of supercooling, consistent with the behavior of our numerical data. Note that the treatment of either anisotropy is neglected in his model.

Another comparison can be made with Brener's analysis. As Brener predicted that $\tilde{v} \sim P^{1/6}$ for case (i) and $\tilde{v} \sim P^{11/2}$ for case (ii), the relations $\sigma \sim P^{-11/6}$ for case (i) and $\sigma \sim P^{7/2}$ for case (ii) can be deduced. In other words, since $P \sim S^2$ for the range of small S he studied, σ decreases with S in case (i) and increases strongly (as S^7) in case (ii). The latter is in contradiction to our results. The difference arises because he predicted a much stronger dependence of the tip radius on supercooling than ours, as we discussed previously.

We also observed that σ increases with either anisotropy. The value of σ was seen to increase with $\bar{m}$ in case (i) and case (iii) and to decrease with $\bar{m}$ in case (ii). Apparently, the functional dependence of σ on $\bar{m}$ is greatly influenced by either anisotropy.

ACKNOWLEDGMENTS

The authors are grateful for discussions with B. T. Murray, A. A. Wheeler, S. R. Coriell, R. J. Braun, and G. B. McFadden. This work was performed with support from the National Science Foundation under Grants Nos. DMR-9211276 and MCA94P008P. The services provided by the Pittsburgh Supercomputing Center are also gratefully acknowledged.

[1] B. Billia and R. Trevedi, in *Handbook of Crystal Growth*, edited by D.T.J. Hurle (North-Holland, Amsterdam, 1993), Vol. 1b, pp. 899–1073; M.E. Glicksman and S.P. Marsh, *ibid.*, pp. 1075–1122.
[2] G.P. Ivantsov, Dokl. Akad. Nauk SSSR, **58**, 567 (1947) [translation by G. Horvay, General Electric Research Report No. 60-RL-2511M, 1960].
[3] J.S. Langer and H. Müller-Krumbhaar, J. Cryst. Growth **42**, 11 (1977).
[4] J.S. Langer and H. Müller-Krumbhaar, Acta Metall. **26**, 1681, (1978), **26**, 1689 (1978); **26**, 1697 (1978).
[5] W.W. Mullins and R.F. Sekerka, J. Appl. Phys. **34**, 323 (1963), **35**, 444 (1964).
[6] D. Kessler, J. Koplik, and H. Levine, Phys. Rev. A **34**, 4980 (1986).
[7] E.A. Brener, Zh. Eksp. Teor. Fiz. **96**, 237 (1989) [Sov. Phys. JETP **69**, 133 (1989)].
[8] E.A. Brener and H. Levine, Phys. Rev. A **43**, 883 (1991).
[9] B. Caroli, C. Caroli, C. Misbah, and B. Roulet, J. Phys. (Paris) **48**, 547 (1987).
[10] A. Barbieri and J.B. Langer, Phys. Rev. A **39**, 5314 (1989).
[11] S. Tanveer, Phys. Rev. A **40**, 4756 (1989).
[12] R.F. Sekerka, J. Cryst. Growth **154**, 377 (1995).
[13] J.S. Langer, in *Chance and Matter*, edited by J. Souletie, J. Vannimenus, and R. Stora (North-Holland, Amsterdam, 1987), p. 629.
[14] D.A. Kessler, J. Koplik, and H. Levine, Adv. Phys. **37**, 255 (1988).
[15] J.S. Langer, Science **243**, 1150 (1989).
[16] E.A. Brener and I. Mel'nikov, Adv. Phys. **40**, 53 (1991).
[17] M.E. Glicksman and N.B. Singh, J. Cryst. Growth **98**, 277 (1989).
[18] E.R. Rubinstein and M.E. Glicksman, J. Cryst. Growth **112**, 84 (1991).
[19] J.H. Bilgram, M. Firmann, and W. Känzig, Phys. Rev. B **37**, 685 (1988).
[20] J. H. Bilgram, M. Firmann, and E. Hurlimann, J. Cryst. Growth **96**, 175 (1989).
[21] J.Q. Broughton and G.H. Gilmer, J. Chem. Phys. **84**, 5759 (1986).
[22] R. Willnecker, D.M. Herlach, and B. Feuerbacher, Phys. Rev. Lett. **62**, 2707 (1989).
[23] J.P. Gollub, in *Asymptotics Beyond All Orders*, edited by H. Segur, S. Tanveer and H. Levine (Plenum, New York, 1991), p. 75.
[24] J.S. Langer (private communication).
[25] J.S. Langer, in *Directions in Condensed Matter Physics*, edited by G. Grinstein and G. Mazenko (World Scientific, Singapore, 1986), p. 165.
[26] J.B. Collins and H. Levine, Phys. Rev. B **31**, 6119 (1985).
[27] G. Caginalp, in *Applications of Field Theory to Statistical Mechanics*, edited by L. Garrido, Lecture Notes in Physics Vol. 216 (Springer, Berlin, 1985), p. 216.
[28] G. Caginalp, in *Material Instabilities in Continuum Problems and Related Mathematical Problems*, edited by J.M. Ball (Oxford University Press, Oxford, 1988), p. 35.
[29] G. Caginalp and P.C. Fife, Phys. Rev. B **33**, 7792 (1986).
[30] G. Caginalp, Arch. Rat. Mach. Anal. **92**, 205 (1986).
[31] G. Caginalp, Ann. Phys. (N.Y.) **172**, 136 (1986).
[32] G. Caginalp and P.C. Fife, SIAM J. Appl. Math. **48**, 506 (1988).
[33] G. Caginalp, Phys. Rev. A **39**, 5887 (1989).
[34] G. Caginalp and E.A. Socolovsky, J. Comput. Phys. **95**, 85 (1991).
[35] G. Caginalp and X. Chen, in *On the Evolution of Phase Boundaries*, edited by M.E. Gurtin and G.B. McFadden, IMA Volumes in Mathematics and Its Applications Vol. 43 (Springer, Berlin, 1992), p. 1.
[36] M.E. Gurtin, in *Metastability and Incompletely Posed Problems*, edited by S. Antman, J.L. Ericksen, D. Kinderlehrer, and I. Muller, IMA Volumes in Mathematics and Its Applications Vol. 3 (Springer, Berlin, 1987), p. 135.
[37] E. Fried and M.E. Gurtin, Physica D **68**, 326 (1993).
[38] E. Fried and M.E. Gurtin, Physica D **72**, 287 (1994).
[39] E. Fried and M.E. Gurtin, (to be published).
[40] P.C. Fife and G.S. Gill, Physica D **35**, 267 (1989).
[41] P.C. Fife and G.S. Gill, Phys. Rev. A **43**, 843 (1991).

[42] A.R. Umantsev and A.L. Roitburd, Fiz. Tverd. Tela (Leningrad) **30**, 1124 (1988) [Sov. Phys. Solid State **30**, 651 (1988)].
[43] A.R. Umantsev, J. Chem. Phys. **96**, 605 (1992).
[44] O. Penrose and P.C. Fife, Physica D **43**, 44 (1990).
[45] O. Penrose and P.C. Fife, Physica D **69**, 107 (1993).
[46] S.-L. Wang, R.F. Sekerka, A.A. Wheeler, B.T. Murray, S.R. Coriell, R.J. Braun, and G.B. McFadden, Physica D **69**, 189 (1993).
[47] G.B. McFadden, A.A. Wheeler, R.J. Braun, S.R. Coriell, and R.F. Sekerka, Phys. Rev. E **48**, 2016 (1993).
[48] H.M. Soner, Arch. Rat. Mech. Anal. **31**, 139 (1995).
[49] P.C. Fife and O. Penrose, Electronic J. Diff. Eqns. 1995, **1** (1995).
[50] R. Kobayashi, Bull. Jpn. Soc. Ind. Appl. Math. **1**, 22 (1991).
[51] R. Kobayashi, in: *Computing Optimal Geometries Proceedings, AMS Special Session*, edited by Jean Taylor, (videotape) (AMS, Providence, 1991).
[52] R. Koyabashi, Physica D **63**, 410 (1993).
[53] A.A. Wheeler, B.T. Murray, and R.J. Schaefer, Physica D **66**, 243 (1993).
[54] B.T. Murray, W.J. Boettinger, G.B. McFadden, and A.A. Wheeler, in *Heat Transfer in Melting, Solidification, and Crystal Growth*, edited by I.S. Habib and S. Thynell (ASME, New York, 1993), p. 67.
[55] G. Caginalp and E. Socolovsky, SIAM J. Sci. Comput. **15**, 106 (1994).
[56] R. Kupferman, O. Shochet, and E. Ben-Jacob, Phys. Rev. E **50**, 1005 (1994).
[57] R. Koyabashi, in *Pattern Formation in Complex Dissipative Systems*, edited by S. Kai (World Scientific, Singapore, 1992), p. 121, and associated videotape.
[58] S.-L. Wang and R.F. Sekerka, J. Comput. Phys. (to be published).
[59] John C. Strickwerda, *Finite Difference Schemes and Partial Differential Equations* (Wadsworth and Brooks, Pacific Grove, CA, 1989).
[60] E.A. Brener and D.E. Temkin, Europhys. Lett. **10**, 171 (1989).
[61] M.E. Gurtin, Arch. Rat. Mech. Anal. **96**, 199 (1986).
[62] E. Ben-Jacob, P. Garik, T. Mueller, and D. Grier, Phys. Rev. A **38**, 1370 (1988).
[63] D. Turnbull, Metall. Trans. A **12**, 693 (1981).